



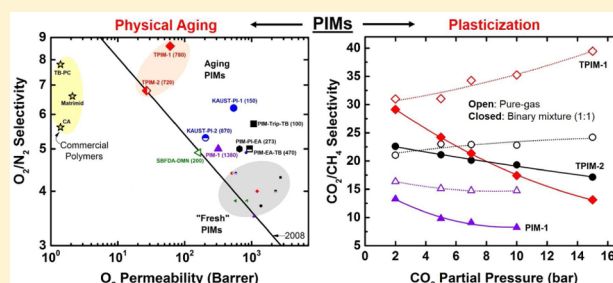
Physical Aging, Plasticization and Their Effects on Gas Permeation in “Rigid” Polymers of Intrinsic Microporosity

Raja Swaidan, Bader Ghanem, Eric Litwiller, and Ingo Pinnau*

Advanced Membranes and Porous Materials Center (AMPMC), Physical Sciences and Engineering Division, King Abdullah University of Science and Technology (KAUST), Al-Jaziri Building 4, Thuwal, 23955-6900, Kingdom of Saudi Arabia

Supporting Information

ABSTRACT: Long-term physical aging and plasticization, two mobility-based phenomena that are counterintuitive in the context of “rigid” polymers of intrinsic microporosity (PIMs), were evaluated using pure- and mixed-gas permeation data for representative ladder and semiladder PIMs. PIMs between 1 and 4 years old retained from 10- to 1000-fold higher H_2 and O_2 permeabilities than commercial membrane materials with similar or higher selectivities. A triptycene-based ladder polymer (TPIM-1) exhibited very large selectivity gains outweighing permeability losses after 780 days, resulting in unprecedented performance for O_2/N_2 ($P(O_2) = 61$ Barrer, $\alpha(O_2/N_2) = 8.6$) and H_2/N_2 ($P(H_2) = 1105$ Barrer, $\alpha(H_2/N_2) = 156$) separations. Interestingly, TPIM-1 aged more and faster than its *more flexible* counterpart, PIM-1, which exhibited $P(O_2) = 317$ Barrer and $\alpha(O_2/N_2) = 5.0$ at 1380 days. Additionally, the more “rigid” TPIM-1 plasticized more significantly than PIM-1 (i.e., TPIM-1 endured $\sim 93\%$ increases in mixed-gas CH_4 permeability over pure-gas values compared to $\sim 60\%$ for PIM-1). A flexible 9,10-bridgehead (i.e., TPIM-2) mitigated the enhancements induced by physical aging but reduced plasticization. Importantly, *intra-chain* rigidity alone, without consideration of chain architecture and *ultra-microporosity*, is insufficient for designing aging- and plasticization-resistant gas separation membranes with high permeability and high selectivity



INTRODUCTION

Polymer membrane technology constitutes a potentially cost-effective and less energy-intensive alternative to conventional gas separation technologies such as distillation and absorption.^{1,2} The criteria for deployment of a polymer into the industrial membrane arena are rigorous.^{3,4} Newly developed polymers should: (i) Demonstrate combinations of permeability and selectivity appropriate for the target separation, (ii) show performance stability over time (typically 3–5 years), (iii) be solution processable, and (iv) be manufacturable into mechanically robust asymmetric or composite membranes with thin and predominantly defect-free selective layers. The difficulty in satisfying all these criteria is reflected in a domination of 90% of the market by less than ten, mostly commercially available, polymers.³

It has been suggested for more than 20 years that polymer structures striking a balance between intrachain mobility and interchain spacing would offer superior gas separation membranes potentially defying state-of-the-art permeability/selectivity trade-offs.^{5–7} Recently developed amorphous and solution-processable polymers of intrinsic microporosity (PIMs), which trap microporosity (IUPAC, <2 nm “pores”) simply by virtue of torsion-resistant and contorted fused-ring backbones that pack inefficiently in the solid state^{8–25} may be one of the most promising classes of materials providing unprecedented gas separation performance. Specifically, previous reports showed that the integration of bridged-bicyclic

contortion centers (i.e., ethanoanthracene, Tröger’s base, triptycene) into fully fused-ring ladder polymers^{10,18,19} and semiladder PIM-polyimides (PIM-PIs)^{11,12,14,16,26} resulted in highly ultramicroporous (<7 Å) PIMs with high selectivities matching those of commercial materials (e.g., polycarbonate, cellulose acetate, Matrimid) but with up to 3 orders of magnitude higher permeabilities, especially in the large-scale industrial applications of nitrogen production from air and hydrogen purification.^{3,4}

One major obstacle to the commercialization of glassy amorphous PIMs for membrane applications is physical aging and the ensuing instability of their permeation properties over time.^{3,27,28} Physical aging in glassy polymers involves a reversible densification driven by a dissipation of non-equilibrium free volume toward an equilibrium state of polymer chain packing. Struik has thermodynamically described the driving force for physical aging—and hence its extent and rate—as being proportional to the difference between the current specific volume (v) and the specific volume at equilibrium (v_∞) (i.e., $dv/dt \propto (v - v_\infty)$).²⁸ Though still not fully understood, it is thought to occur via molecular reorganizations depending on chain mobility.²⁷ For PIMs, this is rather counterintuitive in the context of (i) their “rigid”

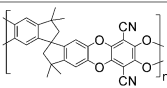
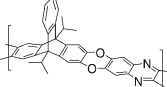
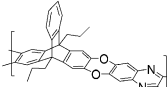
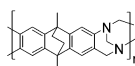
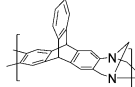
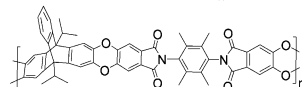
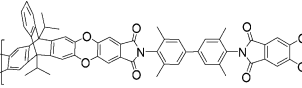
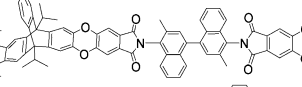
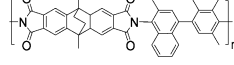
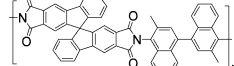
Received: July 17, 2015

Revised: August 11, 2015

Published: August 29, 2015



Table 1. Structure, BET Surface Areas, Thicknesses and Casting Solvents for Representative PIM Films.

Polymer	Structure	BET S.A. (N ₂) (m ² g ⁻¹)	Thickness (μm)	Solvent	Ref.
PIM-1		770	102	CHCl ₃	This work
TPIM-1		860	103	CHCl ₃	This work
TPIM-2		610	46	CHCl ₃	This work
PIM-EA-TB		1030	180	CHCl ₃	18, 19
PIM-Trip-TB		900	132	CHCl ₃	19
KAUST-PI-1		750	77; 102	CHCl ₃	This work
KAUST-PI-2		740	57	CHCl ₃	This work
KAUST-PI-7		840	85	CHCl ₃	This work
PIM-PI-EA		620	72	CHCl ₃	16
SBFDA-DMN		690	123	CHCl ₃	52

chains, (ii) the lack of a measurable T_g , and (iii) the concept that they possess open “pores” with relative permanency on the time-scale of gas transport, unlike traditional solution-diffusion membranes in which transport occurs through *transient* pores forming via thermally activated chain motions.²⁹ However, a body of literature suggests that neither intrachain rigidity (e.g., central to PIM design)^{30,31} nor interchain rigidity (e.g., covalently cross-linked polyimides)^{32,33} have successfully eluded the microstructural rearrangements of physical aging, and that instead the polymers with higher *intra*-chain rigidity aged more and faster. In the broadest rationalization of physical aging, the amount of free volume governs the rate and extent of aging.²⁸ For example, the aging behaviors of two commercial polymers used for membrane separation—Matrimid and polysulfone—were investigated by Rowe et al.³¹ Matrimid has a more torsion-resistant backbone and higher free volume (e.g., more permeable) than polysulfone. However, the extent (e.g., absolute permeability loss) and rate of aging for Matrimid were greater than for polysulfone (PSF) films of similar thickness and treatment history. Likewise, isotropic films of 6FDA-DAM polyimide aged more and faster than similarly treated films of 6FDA-mPDA polyimide despite the greater intrachain rigidity of 6FDA-DAM.³⁰ Again, 6FDA-DAM was the more permeable polymer possessing higher initial free volume.

Plasticization is another important phenomenon that has significant practical implications in membrane-based gas

separation. It is particularly important in natural gas sweetening, one of the fastest growing applications of membrane-based gas separation technology.⁴ As in physical aging, plasticization is based upon molecular chain reorganization of a polymer induced by high sorption of a condensable gas.^{34,35} The resulting selectivity reductions increase product CH₄-loss into a low-pressure permeate and reduce the membrane system’s competitiveness against standard amine absorption columns.^{4,36,37} There have been expectations^{38–40} that state-of-the-art PIMs boasting high intrachain rigidities could demonstrate resilience against plasticization. To date, unlike for physical aging, plasticization has successfully been mitigated with polymers engaging in interchain interactions via (i) high-temperature chemical cross-linking, thermal rearrangement, and carbonization,^{38,41–43} (ii) sub- T_g annealing,^{44–46} and/or (iii) the introduction of hydrogen-bonding moieties.^{14,47–50} Several works have recently reached similar conclusions with ladder PIMs⁴⁹ and PIM-type polyimides (PIM-PIs).^{13,14,51}

The main focus of this work was to investigate how the relatively extreme *intra*-chain rigidity and high ultramicroporosity in some of today’s most permeable and selective PIMs can potentially mitigate long-term physical aging and plasticization, two *mobility*-based phenomena that are counterintuitive in the context of the “rigid” backbones characteristic of PIMs. To address this matter, two sets of permeation data are presented for films of representative ladder PIMs, including the prototypical PIM-1 and semiladder PIM-PIs: (i) long-term

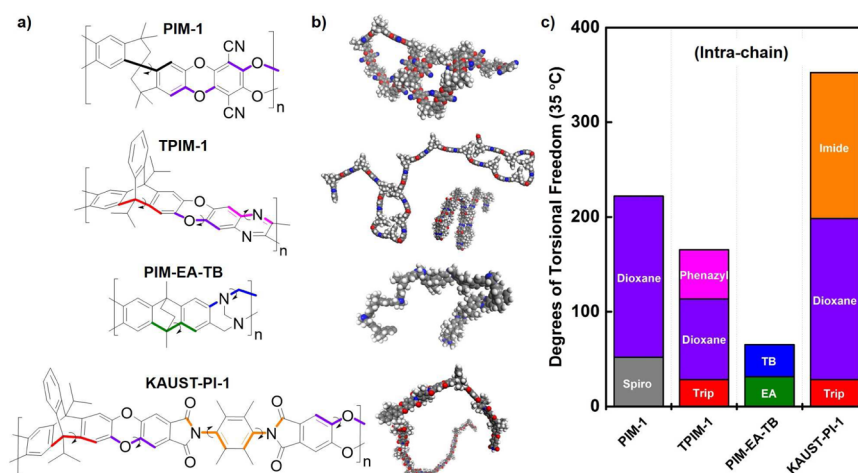


Figure 1. (a) Repeat unit chemical structures, (b) energy-minimized chain conformations (Materials Studio, Accelrys, 7.0), and (c) the degrees of torsional freedom at 35 °C in one repeat unit for several representative PIMs. Torsions were calculated about the color-coded, highlighted bonds in the repeat units.

physical aging data gauged by pure-gas permeabilities and (ii) high-pressure pure- and mixed-gas CO_2/CH_4 separation properties. The permeation data are discussed in terms of relative changes and absolute separation performance to gauge the effects of physical aging and plasticization on the PIMs.

EXPERIMENTAL SECTION

Polymers. Table 1 is a tabulation of names, chemical structures, BET surface areas and the film thicknesses and casting solvents used for some representative ladder PIMs and semiladder PIM-PIs reported in the literature. This work presents new data for thick films of ladder polymers PIM-1, TPIM-1 and TPIM-2 as well as for semiladder PIM-PIs KAUST-PI-2 and KAUST-PI-7, which are shown in comparison to published data for the other polymers.^{16,18,19,52}

Polymer Film Preparation. Solutions containing 3–5 wt % polymer were syringe-filtered with 0.45 μm PTFE filters and cast onto clean, flat-bottomed glass dishes. Clear, isotropic polymer films were obtained by covering the dishes to induce slow evaporation of the casting solvent. The resulting films were dried at 120 °C under vacuum for 12 h, soaked in methanol for 24 h to “reset” their thermal histories and exchange any residual casting solvent, and finally dried at 120 °C under vacuum for 24 h. Removal of the casting solvent was confirmed with thermal gravimetric analysis (TGA, TA Q-5000). Effective areas and thicknesses of the films were determined by calibrated scanning software and a digital micrometer, respectively. All polymers in Table 1 were treated this way except for PIM-EA-TB, PIM-Trip-TB and PIM-PI-EA, which were air-dried after the methanol soak. It is important to note that previous work has demonstrated thickness-dependent physical aging properties for PIMs.⁵³

Molecular Simulations. The repeat units of PIM-1, TPIM-1, PIM-EA-TB, and KAUST-PI-1 were constructed in Materials Studio (Accelrys, 7.0). The conformer module was used to incrementally vary select dihedral angles (bold and color-coded in Figure 1) from -180° to $+180^\circ$. For each conformer, geometry optimizations were performed with the Forcite module using a COMPASS force field and Smart algorithm (fine quality and 50 000 iterations). The energy barriers (kJ/mol) to changes in the dihedral angles were calculated relative to the lowest energy attained ($\Delta E = E_i - E_{\min}$) over the 360° range. The degrees of torsional freedom were then defined as the total number of degrees available for torsion about the color-coded bonds at a temperature T , where the available energy at temperature T was approximated by the equipartition theorem ($\sim 3RT$).⁵⁴ Isolated polymer chains (usually of 10–20 repeat units) were constructed from the repeat units using the polymer builder function. Initially, the chains were constructed with random torsions between the repeat units. The Forcite module (COMPASS force field, Smart algorithm

with fine quality and 50 000 iterations) was then used to obtain the energy-minimized chain conformation of each chain in isolation.

Pure-Gas Permeation Measurements. The pure-gas permeabilities of the films were determined using the constant-volume/variable-pressure method. After drying the methanol-soaked films at 120 °C for 24 h under vacuum, they were immediately masked between two aluminum-tape donuts. On one side, the interface between the film and tape was lightly epoxied using a two-part potting epoxy (GC Electronics) which showed excellent durability over long times. The masked film was degassed in the permeation test apparatus on both sides under high vacuum at 35 °C. Pure gases (grade 5 and above) were fed to the epoxied side at 35 °C and 2 bar. In addition, the CO_2 and CH_4 pure-gas permeabilities were measured at pressures from 2 to 15 bar for TPIM-1 and TPIM-2. The increase in permeate pressure with time was measured by an MKS Baratron transducer. The pure-gas permeabilities were calculated by

$$P = DS = 10^{10} \frac{V_d l}{p_{up} A R T} \frac{dp}{dt}$$

where P is the gas permeability (Barrer) ($1 \text{ Barrer} = 10^{-10} \text{ cm}^3 (\text{STP}) \text{ cm cm}^{-2} \text{ s}^{-1} \text{ cmHg}^{-1}$), p_{up} is the upstream pressure (cmHg), dp/dt is the steady-state permeate-side pressure increase (cmHg s^{-1}), V_d is the calibrated permeate volume (cm^3), l is the membrane thickness (cm), A is the effective membrane area (cm^2), T is the operating temperature (K), and R is the gas constant ($0.278 \text{ cm}^3 \text{ cmHg cm}^{-3} (\text{STP}) \text{ K}^{-1}$). The ideal permselectivity ($\alpha_{A/B}$) for separation of A/B was calculated by

$$\alpha_{A/B}^{\text{ideal}} = \frac{P_A}{P_B}$$

Mixed-Gas Permeation Measurements. The mixed-gas permeation properties for ~ 15 -day-old films were measured at 35 °C with a 50:50 CO_2/CH_4 binary mixture using a setup similar to that previously described by O'Brien et al.⁵⁵ The films were evaluated at total pressures ranging from 4 to 30 bar such that the mixed-gas CO_2 partial pressures were equal to those used in the pure CO_2 permeation experiments. This methodology permits direct comparison of the pure- and mixed-gas data to elucidate any nonidealities including plasticization and competitive sorption. The stage-cut, that is, the ratio of permeate to feed flow rates, was less than 0.01 to ensure that the residue composition was essentially equal to that of the feed gas. CO_2 and CH_4 concentrations were measured with a calibrated gas chromatograph (Agilent 3000A Micro GC) equipped with thermal conductivity detectors. The mixed-gas permeability of component i was determined by

$$P_i = 10^{10} \frac{y_i V_d^l}{x_i p_{up} ART} \frac{dp}{dt}$$

where y and x are the mole fractions in the permeate and feed, respectively, and p_{up} is the upstream partial pressure of component i . Because the downstream pressure was negligible, the mixed-gas selectivity of component i/j was obtained from

$$\alpha_{i/j} = \frac{y_i/y_j}{x_i/x_j}$$

Steady-state permeation was identified at each feed pressure when regular measurements of permeability and selectivity *both* changed negligibly with time.

RESULTS AND DISCUSSION

Molecular Simulations: Intra-Chain “Rigidity” and Chain Architecture. Polymers of intrinsic microporosity are often recognized for their high “rigidity,” a rather general term which is more appropriately referred to here as “intra-chain” rigidity—describing specifically short-range motions including, for example, local torsions within the backbone—to distinguish from “inter-chain” rigidity.⁵¹ Figure 1 qualitatively investigates the intrachain rigidities and chain architectures for several representative polymers as determined via molecular simulation (Materials Studio, Accelrys, 7.0). As expected, the ladder polymers (e.g., PIM-1, TPIM-1, PIM-EA-TB) exhibit considerable reductions in backbone flexibility (i.e., degrees of torsional freedom) over the semiladder polyimide KAUST-PI-1, primarily due to the presence of a torsionable imide-linkage in the latter. Moreover, PIM-EA-TB, a completely fused-ring ladder polymer devoid of any flexible dioxane or phenazyl moieties present in the other polymers, shows the highest intrachain rigidity (i.e., lowest number of degrees of torsional freedom). In addition, Figure 1 highlights key differences in the chain architectures of the PIMs (Figure 1b). Most interestingly, TPIM-1 possesses a unique chain conformation that resembles a *two-dimensional* ribbon-like propagation through space (Figure 1b). This is in stark contrast to the highly contorted and erratic structure of the spiro-centered PIM-1 and even the structures of Tröger’s-base-containing ladder polymers such as PIM-EA-TB, all which exhibit a *three-dimensional* propagation. KAUST-PI-1 chains, as for other polyimides, also propagate in three dimensions owing to a larger amount of torsional freedom about the *N*-phenyl imide bonds (Figure 1c). These observations will be addressed in discussion of the transport properties below.

Pure-Gas Permeation Properties: Long-Term Physical Aging. Long-term physical aging of the polymers presented in Table 1 was characterized with pure-gas permeabilities and summarized in Table 2. Details of testing and storage conditions are provided in the footnotes to Table 2. All the polymers were soaked in methanol to “reset” their thermal histories and remove residual casting solvent. The main differences in the handling of the films were as follows: (i) Data for PIM-EA-TB, PIM-Trip-TB, and PIM-PI-EA were previously reported and collected at 25 °C after *ambient* drying of the methanol-soaked films; (ii) the remainder of the polymers were examined in this work at 35 °C after methanol soaking and then drying for 24 h at 120 °C under vacuum.

On the basis of Table 2, the overall losses in O_2 permeability, $P(O_2)$, and gains in O_2/N_2 selectivity, $\alpha(O_2/N_2)$, over the times investigated are expressed percentage wise in Figure 2. The same is done for H_2 permeability and H_2/N_2 selectivity in

Table 2. Long-Term Physical Aging of PIMs Tracked by Pure-Gas Permeabilities

polymer	age (days)	permeability (Barrer)			selectivity	
		H_2	O_2	N_2	H_2/N_2	O_2/N_2
PIM-1 ^a	1	3623	1076	308	12	3.5
	1380	1544	317	64	24	5.0
TPIM-1 ^b	1	4300	1213	303	14	4.0
	15	3304	525	90	37	5.9
	780	1105	61	7.1	156	8.6
TPIM-2 ^b	1	1010	511	117	9	4.4
	15	737	121	24	31	5.0
	720	354	27	4.0	90	6.8
PIM-EA-TB ^c	1	8114	2294	580	14	4.0
	470	4442	933	188	24	5.0
PIM-Trip-TB ^c	1	8039	2718	629	13	4.3
	100	4740	1073	189	25	5.7
KAUST-PI-1 ^a	1	4183	827	169	25	4.9
	15	3983	627	107	37	5.9
	150	3431	542	87	39	6.2
KAUST-PI-2 ^a	1	2436	582	131	19	4.4
	15	2368	490	98	24	5.0
	870	1255	205	39	32	5.3
KAUST-PI-7 ^a	1	—	865	240	—	3.6
	15	3198	842	225	14	3.7
	660	2164	490	115	19	4.3
PIM-PI-EA ^c	1	4230	1380	369	12	3.7
	273	2860	659	131	22	5.0
SBFDA-DMN ^b	1	2966	850	226	13	3.8
	10	2146	593	143	15	4.1
	200	878	161	33	27	4.9

^aFilm immersed in methanol, dried at 120 °C *in vacuo* for 24 h. Storage: days 1–15, *in vacuo*, 35 °C; days 15+, in a sealed plastic bag at ambient conditions. Permeation properties measured at 35 °C and 2 bar. ^bFilm immersed in methanol, dried at 120 °C *in vacuo* for 24 h. Storage: sealed plastic bag under ambient conditions. Permeation properties measured at 35 °C, 2 bar. ^cFilm immersed in methanol, air-dried in ambient. Storage: ambient conditions. Permeation properties measured at 25 °C, 1 bar.

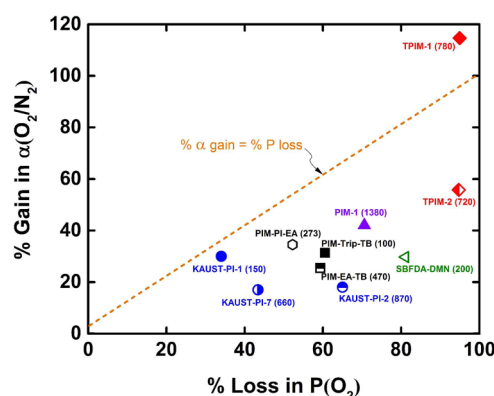


Figure 2. Effects of long-term physical aging on O_2 permeability, $P(O_2)$, and O_2/N_2 selectivity for various PIMs. The number of days aged is shown in parentheses.

Figure 3. Physical aging manifests itself in permeability loss and concomitant selectivity gain, a traditionally observed trade-off.⁵⁶ Furthermore, Figure 2 indicates that the losses in O_2 permeability outweighed the gains in O_2/N_2 selectivity at any length of aging for most of the PIMs. However, hydrogen ($k_D = 2.9$ Å) was less affected by aging-induced physical densification

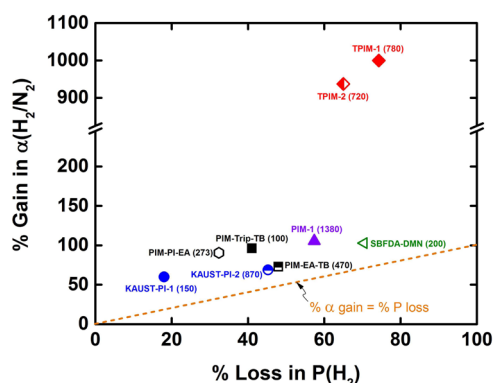


Figure 3. Effects of long-term physical aging on H_2 permeability, $P(H_2)$, and H_2/N_2 selectivity for various PIMs. The number of days aged is shown in parentheses.

than oxygen ($k_D = 3.46 \text{ \AA}$) due to its smaller size, and thus oxygen permeability dropped more with time than hydrogen permeability for any polymer. The gains in H_2/N_2 selectivity thus outweighed the losses in H_2 permeability (Figure 3), as expected. It is important to note that permeability loss in PIMs appears to proceed in two phases. The first phase is documented and characterized by a rapid permeability decline over ~ 15 days and driven by excess nonequilibrium free volume created by methanol soaks.^{12,57,58} At this point, previously termed an “aging-knee,” a slower, more gradual permeability decline occurs that is attributed to a reorganization of the “intrinsic” microporosity. The latter phase is slow due to the restricted mobilities of PIM chains deep in their glassy states (i.e., often no observable T_g).²⁷ However, as indicated by extents of permeability loss and selectivity gain over long times (Table 2 and Figures 2 and 3), significant redistributions in free volume occur in this latter phase. The resulting densification of the microstructure during physical aging reduces both gas diffusivity and solubility coefficients, thereby reducing permeability, but the overall process is diffusion-governed as indicated by the larger changes in both diffusivity and diffusivity selectivity (Table S1, Supporting Information).

There are two particularly interesting observations to be made from Figures 2 and 3, namely (i) an enhanced aging response for TPIM-1 relative to the other PIMs and (ii) a significant effect of the 9,10-triptycene-bridgehead substituent on aging. The first observation is apparent in a comparison of TPIM-1 and PIM-1 films of nearly identical thickness ($\sim 100 \mu\text{m}$) and treatment history. TPIM-1 aged more extensively and faster than PIM-1. PIM-1 lost $\sim 70\%$ in O_2 permeability and gained $\sim 40\%$ in O_2/N_2 selectivity over 1380 days. In comparison, TPIM-1 lost $\sim 95\%$ in O_2 permeability and gained $\sim 115\%$ in O_2/N_2 selectivity over a shorter period of 780 days. Additionally, H_2/N_2 selectivity increased more than 10-fold for TPIM-1, compared to 2-fold for PIM-1. This trend is consistent with prior literature discussed above demonstrating intrachain rigidity to be insufficient in the mitigation of physical aging, and free volume to be the main driving force: That is, TPIM-1 has a more rigid backbone (Figure 1) than PIM-1 and initially higher free volume, the latter indicated by higher N_2 -BET surface areas (860 vs $780 \text{ m}^2 \text{ g}^{-1}$) and higher O_2 permeabilities (1200 vs ~ 1000 Barrer) (Table 2).

The second observation, regarding a significant effect of the 9,10-triptycene-bridgehead substituent on the redistribution of free volume during aging, is apparent in a comparison of TPIM-

1 (isopropyl bridgeheads) and TPIM-2 (propyl bridgeheads) aged for ~ 750 days. TPIM-1 and TPIM-2 both lost $\sim 95\%$ in O_2 permeability, but TPIM-1 gained $\sim 60\%$ more O_2/N_2 selectivity. On the other hand, both lost $\sim 70\%$ in H_2 permeability and acquired similar 9- to 10-fold gains in H_2/N_2 selectivity. These two observations collectively indicate that physical aging in the isopropyl-substituted TPIM-1 significantly affected a narrow range of ultramicroporosity between 3.46 \AA (i.e., O_2 kinetic diameter) and 3.64 \AA (i.e., N_2 kinetic diameter). This is further corroborated by the ~ 2 -fold higher O_2 diffusivity and 30% higher O_2/N_2 diffusivity selectivity in TPIM-1 compared to TPIM-2 (Table S1, Supporting Information). The effect was not as specific in PIM-1 and TPIM-2 where aging more greatly impeded the transport of oxygen, hence the differences in selectivities. The profound role of triptycene’s 9,10-isopropyl-bridgehead on gas sorption in covalent networks⁵⁹ and gas separation in amorphous polymer films^{10,12} has been previously noted, and here it is established as a critical factor in enhancing the molecular sieving function of TPIM-1 during physical aging.

Mechanistically rationalizing the relatively enhanced aging responses of TPIM-1 and TPIM-2 is not trivial. Without overinterpreting the data, the TPIMs trend—more than other similarly aged polymers—toward the upper right corners of Figures 2 and 3, where permeability losses and selectivity gains are quite extensive. Despite only being air-dried after a methanol soak (which should increase the apparent effects of aging), PIM-EA-TB, which has a notably higher chain rigidity (Figure 1), higher free volume due to higher N_2 -BET surface areas (1000 vs $860 \text{ m}^2 \text{ g}^{-1}$) and nearly 2-fold higher initial O_2 permeability (Table 2), does not demonstrate such a drastic aging behavior even by 470 days. Similar behavior was observed for a 660-day old KAUST-PI-7 and 870-day-old KAUST-PI-2. We hypothesize that chain architecture and conformation also play a role in physical aging, potentially by altering the target v_∞ in the context of Struik’s model.²⁸ That is, the unique ribbon-like two-dimensional geometry of energy-minimized TPIM chains (Figure 1) may be more amenable to efficient packing than the more contorted and three-dimensional chain propagations of PIM-EA-TB, PIM-1, etc. That is, a lower v_∞ translates into an increased driving force for aging toward a more efficiently packed equilibrium structure. Along the same lines, what preliminarily appears to be a “mitigated” aging in PIM-EA-TB may be the result of the high concentration of bulky bridged-bicyclic moieties in a fused ring structure that contort the macromolecule in three dimensions and simply increase the v_∞ .

The impact of physical aging on the absolute separation performance of the PIMs is shown in Figures 5 and 6 relative to the 2008 upper bounds⁶⁰ for O_2/N_2 and H_2/N_2 separations, respectively. The smaller symbols within the gray shade represent data taken initially for the “fresh” methanol-treated PIMs (details in footnotes to Table 1). For both separations, the ensuing increases in selectivity and concomitant losses in permeability locate the PIMs well above the 2008 upper bounds to polymer separation performance. Favorably, however, the performance generally transitions from being primarily permeability driven to having a more favorable, balanced contribution of permeability and selectivity. This balance is exemplified by TPIM-1, which exhibits an unprecedented combination of O_2 permeability of 61 Barrer and O_2/N_2 selectivity of 8.6 at 780 days. Relative to a commercially employed air separation material, tetrabromo-polycarbonate

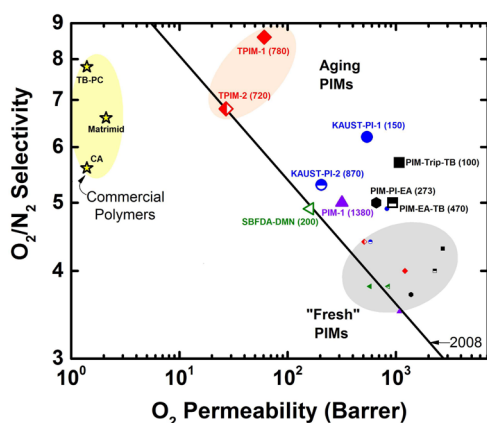


Figure 4. Effects of physical aging on O_2/N_2 separation performance for PIMs. The number of days aged is shown in parentheses. The solid line represents the 2008 upper bound.

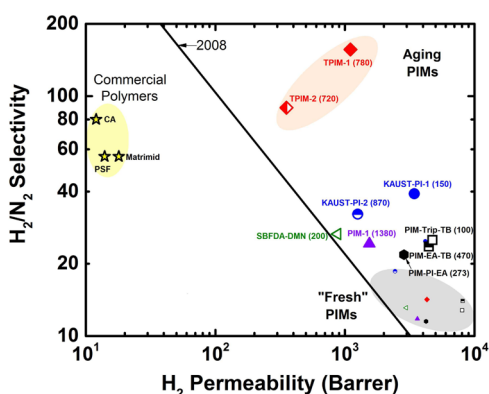


Figure 5. Effects of physical aging on H_2/N_2 separation performance for PIMs. The number of days aged is shown in parentheses. The solid line represents the 2008 upper bound.

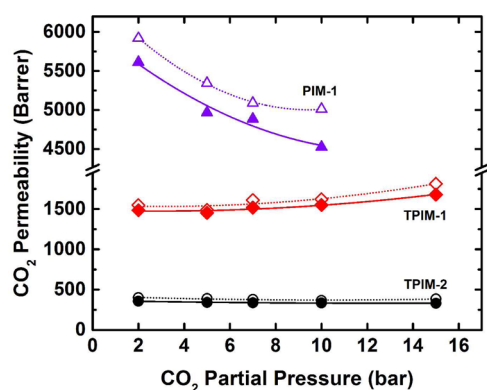


Figure 6. Pressure-dependence of CO_2 permeability isotherms for PIM-1, TPIM-1, and TPIM-2 at 35 °C using a 1:1 CO_2/CH_4 binary feed. Open points, pure gas. Closed points, mixed gas.

(TB-PC) ($P(\text{O}_2) = 1.4$ Barrer, $\alpha(\text{O}_2/\text{N}_2) = 7.8$),⁶¹ TPIM-1 has higher O_2/N_2 selectivity along with ~ 45 -fold higher O_2 permeability. Given the current membrane infrastructure and employed pressure ratios, an O_2/N_2 selectivity of ~ 8 is optimal but higher permeability is particularly advantageous.^{4,62} A similar argument is also apparent for H_2/N_2 separation for both TPIM-1 and TPIM-2, where TPIM-1 offers an outstanding H_2/N_2 selectivity of 156 with an H_2 permeability of 1105 Barrer—that is, a selectivity that matches those of commercially

employed membranes and a permeability that is orders of magnitude higher.⁶² Accordingly, *intra-chain* rigidity alone—which is a main target of standard PIM design—is insufficient in the design of highly permeable and highly selective gas separation membranes with PIMs.

Pressure Dependence of Pure- and Mixed-gas CO_2/CH_4 Permeation Properties: Plasticization. To date, very few reports exist on the plasticization behavior of ladder PIMs⁴⁹ and semiladder PIM-PIs^{13,14,51} under CO_2 -containing mixed-gas feeds. These studies indicated that structural changes increasing interchain rigidity (i.e., between chains) were required to improve plasticization resistance. This was established either via the introduction of (i) hydrogen bonding moieties, (ii) intrachain flexibility that facilitates coplanarization over the *N*-phenyl imide bonds of polyimides and thus the formation of interchain charge-transfer-complexes (CTCs), and (iii) a combination thereof. Moreover, it has been recommended that polymers having lower free volume—typically induced by the aforementioned changes—are better choices for CO_2/CH_4 separation because they sorb less of the plasticizing CO_2 gas.⁶³

It remains interesting, however, to investigate the plasticization behavior of TPIM-1, which possesses a significantly higher intrachain rigidity and molecular sieving character than previously reported PIM-1 and KAUST-PI-1 (Figure 1). Given the large impacts on gas permeation properties of the 9,10-bridgehead substituent on triptycene, as shown above and elsewhere,¹² TPIM-2 was also evaluated. Pure- and mixed-gas (1:1 feed) permeability isotherms spanning (partial) CO_2 pressures of 15 bar are presented for CO_2 and CH_4 in Figures 6 and 7, respectively. In general, lower CO_2 permeabilities

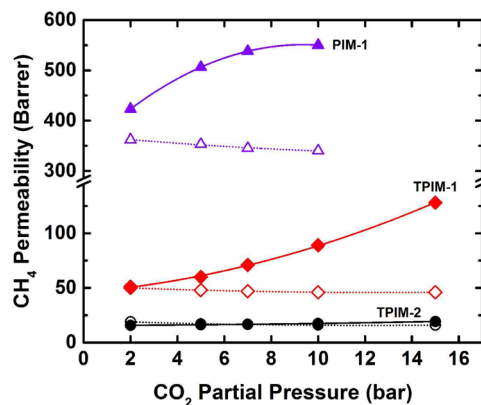


Figure 7. Pressure-dependence of CH_4 permeability isotherms for PIM-1, TPIM-1 and TPIM-2 at 35 °C using a 1:1 CO_2/CH_4 binary feed. Open points, pure gas. Closed points, mixed gas.

under the mixed-gas than the pure-gas conditions are expected due to competitive sorption with CH_4 . The CO_2 permeabilities in PIM-1 exhibited pressure-dependent drops due to dual-mode reductions in the solubility coefficient of CO_2 with pressure, whereas those in the TPIMs were nearly constant or only slightly increased with pressure, preliminarily indicating a small degree of plasticization. However, the only unambiguous indicator of plasticization is the mixed-gas permeability of the slower CH_4 gas (Figure 6). At 10 bar CO_2 partial pressure, TPIM-1 and PIM-1 endured 93% and 62% increases in mixed-gas CH_4 permeability over the pure-gas permeability. TPIM-1 plasticized appreciably more than PIM-1, indicating that greatly

increased intrachain rigidity does *not* inhibit CO₂-induced plasticization, which remains consistent with the literature.⁵¹ Accordingly, the CO₂/CH₄ mixed-gas selectivity in TPIM-1 dropped $\sim 60\%$ in the mixed-gas from ~ 30 at 2 bar to ~ 13 at 10 bar CO₂ partial pressure (Figure 8).

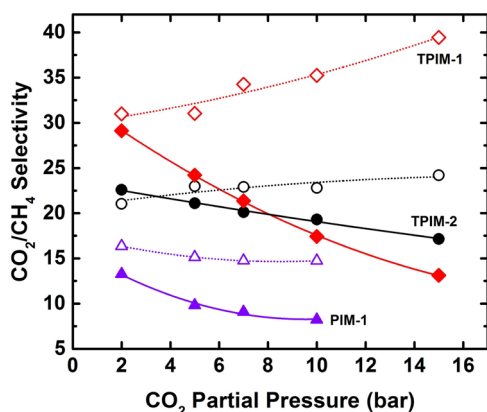


Figure 8. Pressure-dependence of CO₂/CH₄ selectivity isotherms for PIM-1, TPIM-1, and TPIM-2 at 35 °C using a 1:1 CO₂:CH₄ binary feed. Open points, pure gas. Closed points, mixed gas.

It is worth noting the effect of the bridgehead on TPIM plasticization. TPIM-2 plasticized significantly less than TPIM-1 given less than 10% increases in CH₄ mixed-gas permeability over the pure-gas value (Figure 7). It accordingly maintains a higher mixed-gas selectivity (~ 18) at 30 bar total pressure. In a recent paper, a highly ultramicroporous, sieving pore structure akin to that of TPIM-1 was argued to render KAUST-PI-1 (i.e., TMPD diamine) *more vulnerable* to CO₂-induced plasticization than KAUST-PI-5 (i.e., 6FpDA diamine), a relatively flexible polymer with lower permeabilities and lower selectivities.⁵¹ The same hypothesis is corroborated here and described schematically in Figure 9. Briefly, given the combination of high O₂/N₂ selectivity and high O₂ permeability in TPIM-1, a significant portion of its ultramicroporosity is likely dimensioned around O₂ and N₂ at 3–4 Å. This is additionally supported by the unique increases in diffusivity-governed (Table S1) O₂/N₂ sieving behavior observed during physical aging (e.g., time-

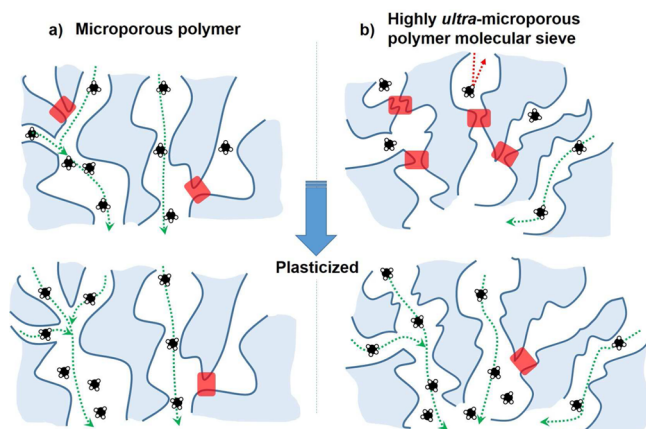


Figure 9. Schematic envisioning a greater “sensitivity” of CH₄ gas transport to CO₂-induced plasticization in a highly ultramicroporous PIM structure. The shaded areas (red) indicate pathways too narrow for the gas to pass.

dependence of pure-gas permeabilities). The envisioned dilation of these 3–4 Å pores during pressure-dependent CO₂/CH₄ testing would *also* impact CO₂ permeability, since CO₂ has an effective size (based on diffusivity, ~ 3.5 – 3.6 Å) between that of O₂ (3.46 Å) and N₂ (3.64 Å).⁶⁴ This is indeed indicated by the strong rises in CO₂ permeability isotherms (Figure 6 and 7) with pressure for TPIM-1, but not for PIM-1 or TPIM-2 (i.e., in which O₂/N₂ transport data indicate such pores do not contribute as significantly to gas transport as in TPIM-1). Furthermore, an even larger impact is envisioned on the diffusion of the larger CH₄ ($k_D = 3.8$ Å) gas especially in a highly ultramicroporous polymer sieve that contains more of the 3.4–3.6 Å pores (Figure 9).

Finally, the CO₂/CH₄ separation performance of notable PIMs is presented in Figure 10 on a permeability/selectivity

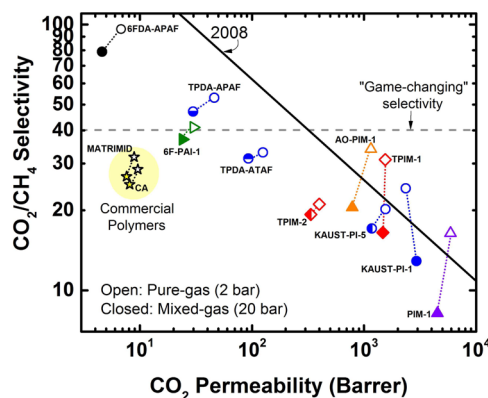


Figure 10. Effects of CO₂-induced plasticization on pure- and mixed-gas CO₂/CH₄ separation performance for PIMs. The solid line represents the 2008 upper bound. The dashed line represents a practically relevant “selectivity” of 40. Open points, pure-gas feeds at 2 bar, 35 °C. Closed points, mixed-gas feeds at 20 bar, 35 °C.

performance map. Data from 2 bar pure-gas measurements (open points) are compared against data from 20 bar 1:1 mixed-gas measurements (closed points) to emphasize the impact of nonideal phenomena including plasticization and competitive sorption on performance. Recently, Baker has defined a mixed-gas selectivity of 40 as critical for membrane technology to outcompete standard amine absorption columns.^{4,65} Briefly, PIMs classically designed with intrachain rigidity (e.g., PIM-1, TPIM-1, TPIM-2, KAUST-PI-1) offer higher permeabilities than commercial materials—which will drop with aging—at the expense of lower mixed-gas CO₂/CH₄ selectivity. Instead, PIMs that integrate interchain interactions (e.g., TPDA-APAF)^{14,66} may retain a permeability edge over commercial materials while still meeting the selectivity target.

CONCLUSIONS

The results reported herein provide a critical perspective on the effects of physical aging and plasticization on a rapidly emerging class of promising polymers, PIMs. Apparently, the very intrachain rigidity that offers PIMs their attractive high-free-volume, ultramicroporous gas sieving microstructures also increases their vulnerability to physical aging and plasticization, both viewed as obstacles for commercialization. However, physical aging induces a favorable transition from permeability-driven gas transport properties to balanced combinations of permeability and selectivity that are outstanding relevant to both the “upper-bound” metric and the performance of

commercially employed polymers. The major conclusions of the work are summarized as follows:

- 1 Physical aging occurs in all PIMs despite their high intrachain rigidities. In fact, the initially high free volume created by greater backbone rigidity serves as a driving force for more extensive and rapid physical aging of the bulk microstructure.
- 2 The inherent chain architecture may be an important consideration in physical aging. Simulations indicate that TPIM macromolecules propagate through space in two-dimensional (i.e., in one plane) ribbon-like conformations, starkly different from the more erratic conformations PIMs usually assume. TPIMs may be able to reach a denser equilibrium chain packing, which would be consistent with the significantly improved molecular sieving behaviors of aged TPIMs.
- 3 Higher intrachain rigidity, central to PIM design and exemplified in the TPIMs studied herein, does not alone prevent plasticization. On the contrary, a highly O₂/N₂ sieving ultramicroporous structure—to which intrachain rigidity is key—appears to be more vulnerable to CO₂-induced plasticization (i.e., as gauged by increases in mixed-gas CH₄ permeabilities under 1:1 CO₂/CH₄ feeds).

Work is currently underway to develop PIM-like structures that are more resilient against physical aging and plasticization. For cases where aging is unavoidable, techniques to accelerate it and improve the stability of the permeation properties with time are needed.

■ ASSOCIATED CONTENT

■ Supporting Information

The Supporting Information is available free of charge on the ACS Publications website at DOI: 10.1021/acs.macromol.5b01581.

Table of long-term aging data and figures showing the effects of long-term physical aging (PDF)

■ AUTHOR INFORMATION

Corresponding Author

*Telephone: +966-12-808-2406 E-mail: ingo.pinnau@kaust.edu.sa (I.P.).

Notes

The authors declare no competing financial interest.

■ ACKNOWLEDGMENTS

The authors acknowledge financial support of this work by KAUST funding for I.P. (BAS/1/1323-01-0).

■ REFERENCES

- (1) Sanders, D. E.; Smith, Z. P.; Guo, R. L.; Robeson, L. M.; McGrath, J. E.; Paul, D. R.; Freeman, B. D. *Polymer* **2013**, *54*, 4729–4761.
- (2) *Materials research for separations technologies: energy and emission reduction opportunities*; US Department of Energy: Washington, DC; USA, 2004; http://www1.eere.energy.gov/manufacturing/industries_technologies/imf/pdfs/separationsreport.pdf
- (3) Baker, R. W.; Low, B. T. *Macromolecules* **2014**, *47*, 6999–7013.
- (4) Baker, R. W. *Ind. Eng. Chem. Res.* **2002**, *41*, 1393–1411.
- (5) Kim, T. H.; Koros, W. J.; Husk, G. R.; O'Brien, K. C. *J. Membr. Sci.* **1988**, *37*, 45–62.

- (6) Stern, S. A.; Mi, Y.; Yamamoto, H.; St Clair, A. K. *J. Polym. Sci., Part B: Polym. Phys.* **1989**, *27*, 1887–1909.
- (7) Freeman, B. D. *Macromolecules* **1999**, *32*, 375–380.
- (8) McKeown, N. B. *ISRN Materials Science* **2012**, *2012*, 513986.
- (9) Budd, P. M.; Ghanem, B. S.; Makhseed, S.; McKeown, N. B.; Msayib, K. J.; Tattershall, C. E. *Chem. Commun.* **2004**, 230–231.
- (10) Ghanem, B. S.; Swaidan, R.; Ma, X.; Litwiller, E.; Pinnau, I. *Adv. Mater.* **2014**, *26*, 6696–6700.
- (11) Ghanem, B. S.; Swaidan, R.; Litwiller, E.; Pinnau, I. *Adv. Mater.* **2014**, *26*, 3688–3692.
- (12) Swaidan, R.; Al-Saeedi, M.; Ghanem, B.; Litwiller, E.; Pinnau, I. *Macromolecules* **2014**, *47*, 5104–5114.
- (13) Ma, X. H.; Swaidan, R.; Belmabkhout, Y.; Zhu, Y. H.; Litwiller, E.; Jouiad, M.; Pinnau, I.; Han, Y. *Macromolecules* **2012**, *45*, 3841–3849.
- (14) Swaidan, R.; Ghanem, B.; Litwiller, E.; Pinnau, I. *J. Membr. Sci.* **2015**, *475*, 571–581.
- (15) Ghanem, B. S.; McKeown, N. B.; Budd, P. M.; Al-Harbi, N. M.; Fritsch, D.; Heinrich, K.; Starannikova, L.; Tokarev, A.; Yampolskii, Y. *Macromolecules* **2009**, *42*, 7881–7888.
- (16) Rogan, Y.; Malpass-Evans, R.; Carta, M.; Lee, M.; Jansen, J. C.; Bernardo, P.; Clarizia, G.; Tocci, E.; Friess, K.; Lanc, M.; McKeown, N. B. *J. Mater. Chem. A* **2014**, *2*, 4874–4877.
- (17) Rogan, Y.; Starannikova, L.; Ryzhikh, V.; Yampolskii, Y.; Bernardo, P.; Bazzarelli, F.; Jansen, J. C.; McKeown, N. B. *Polym. Chem.* **2013**, *4*, 3813–3820.
- (18) Carta, M.; Malpass-Evans, R.; Croad, M.; Rogan, Y.; Jansen, J. C.; Bernardo, P.; Bazzarelli, F.; McKeown, N. B. *Science* **2013**, *339*, 303–307.
- (19) Carta, M.; Croad, M.; Malpass-Evans, R.; Jansen, J. C.; Bernardo, P.; Clarizia, G.; Friess, K.; Lanč, M.; McKeown, N. B. *Adv. Mater.* **2014**, *26*, 3526–3531.
- (20) Bezzu, C. G.; Carta, M.; Tonkins, A.; Jansen, J. C.; Bernardo, P.; Bazzarelli, F.; McKeown, N. B. *Adv. Mater.* **2012**, *24*, 5930–5933.
- (21) Ghanem, B. S.; McKeown, N. B.; Budd, P. M.; Selbie, J. D.; Fritsch, D. *Adv. Mater.* **2008**, *20*, 2766–2771.
- (22) Ghanem, B. S.; McKeown, N. B.; Budd, P. M.; Fritsch, D. *Macromolecules* **2008**, *41*, 1640–1646.
- (23) Guiver, M. D.; Lee, Y. M. *Science* **2013**, *339*, 284–285.
- (24) Jue, M. L.; Lively, R. P. *React. Funct. Polym.* **2015**, *86*, 88–110.
- (25) Maier, G. *Angew. Chem., Int. Ed.* **2013**, *52*, 4982–4984.
- (26) Zhuang, Y. B.; Seong, J. G.; Do, Y. S.; Jo, H. J.; Cui, Z.; Lee, J.; Lee, Y. M.; Guiver, M. D. *Macromolecules* **2014**, *47*, 3254–3262.
- (27) Hutchinson, J. M. *Prog. Polym. Sci.* **1995**, *20*, 703–760.
- (28) Struik, L. C. E. *Polym. Eng. Sci.* **1977**, *17*, 165–173.
- (29) Wijmans, J. G.; Baker, R. W. *J. Membr. Sci.* **1995**, *107*, 1–21.
- (30) Cui, L. L.; Qiu, W. L.; Paul, D. R.; Koros, W. J. *Polymer* **2011**, *52*, 3374–3380.
- (31) Rowe, B. W.; Freeman, B. D.; Paul, D. R. *Polymer* **2009**, *50*, 5565–5575.
- (32) Cui, L. L.; Qiu, W. L.; Paul, D. R.; Koros, W. J. *Polymer* **2011**, *52*, 5528–5537.
- (33) Wang, H.; Chung, T. S.; Paul, D. R. *J. Membr. Sci.* **2014**, *458*, 27–35.
- (34) Wessling, M.; Schoeman, S.; van der Boomgaard, T.; Smolders, C. A. *Gas Sep. Purif.* **1991**, *5*, 222–228.
- (35) Wessling, M.; Huisman, I.; Boomgaard, T. v. d.; Smolders, C. A. *J. Appl. Polym. Sci.* **1995**, *58*, 1959–1966.
- (36) Bhidé, B. D.; Stern, S. A. *J. Membr. Sci.* **1993**, *81*, 209–237.
- (37) Bhidé, B. D.; Stern, S. A. *J. Membr. Sci.* **1993**, *81*, 239–252.
- (38) Xiao, Y.; Low, B. T.; Hosseini, S. S.; Chung, T. S.; Paul, D. R. *Prog. Polym. Sci.* **2009**, *34*, 561–580.
- (39) Chern, R. T.; Koros, W. J.; Sanders, E. S.; Yui, R. *J. Membr. Sci.* **1983**, *15*, 157–169.
- (40) Du, N. Y.; Park, H. B.; Dal-Cin, M. M.; Guiver, M. D. *Energy Environ. Sci.* **2012**, *5*, 7306–7322.
- (41) Vu, D. Q.; Koros, W. J.; Miller, S. J. *Ind. Eng. Chem. Res.* **2002**, *41*, 367–380.

- (42) Park, H. B.; Jung, C. H.; Lee, Y. M.; Hill, A. J.; Pas, S. J.; Mudie, S. T.; Van Wagner, E.; Freeman, B. D.; Cookson, D. J. *Science* **2007**, *318*, 254–258.
- (43) Swaidan, R.; Ma, X. H.; Litwiller, E.; Pinnau, I. *J. Membr. Sci.* **2013**, *447*, 387–394.
- (44) Bos, A.; Punt, I. G. M.; Wessling, M.; Strathmann, H. *Sep. Purif. Technol.* **1998**, *14*, 27–39.
- (45) Zhou, F. B.; Koros, W. J. *Polymer* **2006**, *47*, 280–288.
- (46) Das, M.; Koros, W. J. *J. Membr. Sci.* **2010**, *365*, 399–408.
- (47) Vaughn, J. T.; Koros, W. J.; Johnson, J. R.; Karvan, O. *J. Membr. Sci.* **2012**, *401–402*, 163–174.
- (48) Kraftschik, B.; Koros, W. J.; Johnson, J. R.; Karvan, O. *J. Membr. Sci.* **2013**, *428*, 608–619.
- (49) Swaidan, R.; Ghanem, B. S.; Litwiller, E.; Pinnau, I. *J. Membr. Sci.* **2014**, *457*, 95–102.
- (50) Wind, J. D.; Sirard, S. M.; Paul, D. R.; Green, P. F.; Johnston, K. P.; Koros, W. J. *Macromolecules* **2003**, *36*, 6433–6441.
- (51) Swaidan, R.; Ghanem, B.; Al-Saeedi, M.; Litwiller, E.; Pinnau, I. *Macromolecules* **2014**, *47*, 7453–7462.
- (52) Ma, X.; Ghanem, B.; Salines, O.; Litwiller, E.; Pinnau, I. *ACS Macro Lett.* **2015**, *4*, 231–235.
- (53) Tiwari, R. R.; Smith, Z. P.; Lin, H.; Freeman, B. D.; Paul, D. R. *Polymer* **2014**, *55*, 5788–5800.
- (54) Mi, Y.; Stern, S. A.; Trohalaki, S. *J. Membr. Sci.* **1993**, *77*, 41–48.
- (55) O'Brien, K. C.; Koros, W. J.; Barbari, T. A.; Sanders, E. S. *J. Membr. Sci.* **1986**, *29*, 229–238.
- (56) Pfromm, P. H. The Impact of Physical Aging of Amorphous Glassy Polymers on Gas Separation Membranes. In *Materials Science of Membranes for Gas and Vapor Separation*; John Wiley & Sons, Ltd.: London, 2006; pp 293–306.
- (57) Hill, A. J.; Pas, S. J.; Bastow, T. J.; Burgar, M. I.; Nagai, K.; Toy, L. G.; Freeman, B. D. *J. Membr. Sci.* **2004**, *243*, 37–44.
- (58) Budd, P. M.; McKeown, N. B.; Ghanem, B. S.; Msayib, K. J.; Fritsch, D.; Starannikova, L.; Belov, N.; Sanfirova, O.; Yampolskii, Y.; Shantarovich, V. *J. Membr. Sci.* **2008**, *325*, 851–860.
- (59) Ghanem, B. S.; Hashem, M.; Harris, K. D. M.; Msayib, K. J.; Xu, M. C.; Budd, P. M.; Chaukura, N.; Book, D.; Tedds, S.; Walton, A.; McKeown, N. B. *Macromolecules* **2010**, *43*, 5287–5294.
- (60) Robeson, L. M. *J. Membr. Sci.* **2008**, *320*, 390–400.
- (61) Hellums, M. W.; Koros, W. J.; Husk, G. R.; Paul, D. R. *J. Appl. Polym. Sci.* **1991**, *43*, 1977–1986.
- (62) Baker, R. W. *Membrane Technology and Applications*, 2nd ed.; John Wiley & Sons, Ltd.: London, 2004.
- (63) Koros, W. J.; Walker, D. R. B. *Polym. J.* **1991**, *23*, 481–490.
- (64) Robeson, L. M.; Smith, Z. P.; Freeman, B. D.; Paul, D. R. *J. Membr. Sci.* **2014**, *453*, 71–83.
- (65) Baker, R. W.; Lokhandwala, K. *Ind. Eng. Chem. Res.* **2008**, *47*, 2109–2121.
- (66) Du, N. Y.; Park, H. B.; Robertson, G. P.; Dal-Cin, M. M.; Visser, T.; Scoles, L.; Guiver, M. D. *Nat. Mater.* **2011**, *10*, 372–375.